

Unconventional photon blockade in a three-mode system with double second-order nonlinear coupling

Hong-Yu Lin(林宏宇), Hui Yang(杨慧), and Zhi-Hai Yao(姚治海)
Citation: Chin. Phys. B, 2020, 29 (**12**): 120304. DOI: 10.1088/1674-1056/abab82
Journal homepage: http://cpb.iphy.ac.cn; http://iopscience.iop.org/cpb

What follows is a list of articles you may be interested in

Extended Bell inequality and maximum violation

Yan Gu(古燕), Haifeng Zhang(张海峰), Zhigang Song(宋志刚), Jiuqing Liang(梁九卿), Lianfu Wei(韦联福)
Chin. Phys. B, 2018, 27 (**10**): 100303. DOI: 10.1088/1674-1056/27/10/100303

Superconducting phase qubits with shadow-evaporated Josephson junctions

Fei-Fan Su(宿非凡), Wei-Yang Liu(刘伟洋), Hui-Kai Xu(徐晖凯), Hui Deng(邓辉), Zhi-Yuan Li(李志远), Ye Tian(田野), Xiao-Bo Zhu(朱晓波), Dong-Ning Zheng(郑东宁), Li Lv(吕力), Shi-Ping Zhao(赵士平)
Chin. Phys. B, 2017, 26 (**6**): 060308. DOI: 10.1088/1674-1056/26/6/060308

Entanglement and non-Markovianity of a multi-level atom decaying in a cavity

Zi-Long Fan(范子龙), Yu-Kun Ren(任玉坤), Hao-Sheng Zeng(曾浩生)
Chin. Phys. B, 2016, 25 (**1**): 010303. DOI: 10.1088/1674-1056/25/1/010303

Frequency-tunable transmon in a three-dimensional copper cavity

Pan Jia-Zheng, Cao Zhi-Min, Fan Yun-Yi, Zhou Yu, Lan Dong, Liu Yu-Hao, Chen Zhi-Ping, Li Yong-Chao, Cao Chun-Hai, Xu Wei-Wei, Kang Lin, Chen Jian, Yu Hai-Feng, Yu Yang, Sun Guo-Zhu, Wu Pei-Heng
Chin. Phys. B, 2015, 24 (**11**): 110301. DOI: 10.1088/1674-1056/24/11/110301

Spectroscopy and coherent manipulation of single and coupled flux qubits

Wu Yu-Lin, Deng Hui, Huang Ke-Qiang, Tian Ye, Yu Hai-Feng, Xue Guang-Ming, Jin Yi-Rong, Li Jie, Zhao Shi-Ping, Zheng Dong-Ning
Chin. Phys. B, 2013, 22 (**9**): 090312. DOI: 10.1088/1674-1056/22/9/090312

Unconventional photon blockade in a three-mode system with double second-order nonlinear coupling*

Hong-Yu Lin(林宏宇)[1,2], Hui Yang(杨慧)[1], and Zhi-Hai Yao(姚治海)[1,†]

[1] Department of Physics, Changchun University of Science and Technology, Changchun 130022, China
[2] College of Physics and Electronic Information, Baicheng Normal University, Baicheng 137000, China

(Received 14 June 2020; revised manuscript received 16 July 2020; accepted manuscript online 1 August 2020)

The unconventional photon blockade (UPB) for low-frequency mode is investigated in a three-mode system with double second-order nonlinearity. By analyzing the Hamiltonian of the system, the optimal analytic condition of UPB in low-frequency mode is obtained. The numerical results are calculated by solving the master equation in a truncated Fock space, which agrees well with the analytic conditions. Through the numerical analysis of the system, it is found that the weak driving strength is favorable for the system to realize the UPB effect, and the system is insensitive to the changes of attenuation rate and environmental temperature. The comparison with the two-mode system and another similar three-mode system shows that, under similar system parameters, the UPB effect of this double two-order nonlinear system is more obvious.

Keywords: unconventional photon blockade, second-order nonlinearity, quantum interference

PACS: 03.67.Hk, 14.70.Bh, 42.50.–p, 42.60.–v **DOI:** 10.1088/1674-1056/abab82

1. Introduction

A single-photon source is a device that can emit photons one by one, which plays a key role in the realization of quantum information processing and quantum communication.[1–3] Therefore, the realization of single photon source has become a popular research topic in the field of quantum optics.[4,5] At present, a method called photon blockade (PB)[6,7] is one of the main means to realize single-photon control which means that only a single photon is allowed to exist in a nonlinear semiconductor microcavity, that is, the existence of the first photon will hinder the entry of the second photon. And it has been proved experimentally that PB can be achieved in cavity quantum electrodynamics (QED) or circuit-QED.[8] According to the present researches, PB has great application prospects in many fields, such as nonlinear optics,[9–11] photodynamic devices.[12–17]

In theory, there are two physical mechanisms for implementing PB. One is the photon blockade caused by the splitting of energy levels due to the strong nonlinearity of the system, which is called conventional photon blockade (CPB).[18,19] At present, CPB has been applied in cavity-QED,[20] quantum optical systems and second-order nonlinear semiconductor microcavities.[21–24] Moreover, studies have shown that CPB has its application value in the fields of single-photon transistor,[25] interferometer,[26] and quantum optical rectifier.[27,28] Another PB phenomenon was discovered by Liew and Savona in a photon molecule system.[29] Its basic principle is destructive quantum interference between different drive dissipation paths, and it is called unconventional photon blockade (UPB). It is shown that strong antibunching can be realized in two coupled cavities with weak nonlinearities. Under this mechanism, UPB has been realized successively in many weak nonlinear coupling systems.[30–35] With the further development of this field, UPB has also been realized in bidirectional optical cavity quantum dot,[36] polaritonic coupling system,[37] coupled optical machine position system,[38] and single-mode cavity coupled with second-order or third-order nonlinear system.[39–41] Moreover, the non-classical optical statistics of exciton polarization field also depend on UPB.[42] Recently, in Ref. [43], unconventional photon blockade is studied in a two-mode system, and the conditions for strong photon anti-bundling in low-frequency mode are obtained.

In this paper, we investigate the unconventional photon blockade in a three-mode system contains double second-order nonlinear coupling. The optimal condition for strong antibunching is found in the low-frequency mode by analytical calculation and discussion of the optimal condition is presented. By comparing the numerical and analytical solutions, we find that they are in good agreement. By the analysis of numerical solutions, we find that the weak driving strength is favorable for the system to realize the UPB effect, and the system is insensitive to the changes of attenuation rate and envi-

*Project supported by the National Natural Science Foundation of China (Grant No. 11647054) and the Natural Science Foundation of Jilin Province, China (Grant No. JJKH20181088KJ).

†Corresponding author. E-mail: yaozh@cust.edu.cn

© 2020 Chinese Physical Society and IOP Publishing Ltd

ronmental temperature. By comparing it with the two-mode system and another similar three-mode system, we find that the UPB effect is more obvious in current system.

The remainder of this paper is organized as follows: In Section 2, we introduce the physical model of the double second-order nonlinear coupling system. In Section 3, by analytical calculation, we derive an expression for the optimized antibunching, and we give a numerical result and compare it with the analytical one. Not only that, we compare the current system with the two-mode nonlinear system and find the advantages of the system. Conclusions are given in Section 4.

2. Physical model of the double second-order nonlinear coupling system

In this paper we study the unconventional photon blockade in double second-order nonlinear coupling system, which consists of two high-frequency cavities 1 and 3 with frequencies ω_a and ω_c, and one low-frequency cavity 2 with frequency ω_b. The three cavities are coupled by two-order nonlinear $\chi^{(2)}$ materials that mediates the conversion of the single-photon in cavity 1 or cavity 3 into two-photon in cavity 2, and the system model diagram is shown in Fig. 1.

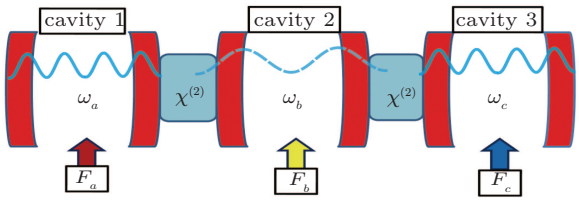


Fig. 1. The scheme of the system consisting of two high-frequency cavities 1 and 3 with frequencies ω_a and ω_c, and one low-frequency cavity 2 with frequency ω_b. The coupling between cavities is by $\chi^{(2)}$ nonlinear material. F_a, F_b, and F_c are the driving strengths for cavities 1, 2, and 3, respectively.

External weak drive is the key to realize UPB, and in this system we choose three-mode drivings. The Hamiltonian of the system can be written as[34]

$$\begin{aligned}\hat{H} = {} & \omega_a\hat{a}^\dagger\hat{a} + \omega_b\hat{b}^\dagger\hat{b} + \omega_c\hat{c}^\dagger\hat{c} + J(\hat{a}^\dagger\hat{b}^2 + \hat{b}^{\dagger 2}\hat{a}) \\ & + g(\hat{c}^\dagger\hat{b}^2 + \hat{b}^{\dagger 2}\hat{c}) + F_a(\hat{a}^\dagger \mathrm{e}^{-\mathrm{i}2\omega_L t} + \hat{a}\mathrm{e}^{\mathrm{i}2\omega_L t}) \\ & + F_b(\hat{b}^\dagger \mathrm{e}^{-\mathrm{i}\omega_L t} + \hat{b}\mathrm{e}^{\mathrm{i}\omega_L t}) + F_c(\hat{c}^\dagger \mathrm{e}^{-\mathrm{i}2\omega_L t} + \hat{c}\mathrm{e}^{\mathrm{i}2\omega_L t}). \quad (1)\end{aligned}$$

Here the $\hat{a}$ ($\hat{a}^\dagger$), $\hat{b}$ ($\hat{b}^\dagger$), and $\hat{c}$ ($\hat{c}^\dagger$) denote the annihilation (creation) operators of fields in the three cavities. The F_a, F_b, and F_c express the driving strengths for the three cavities, while the driving frequencies of F_a and F_c are $2\omega_L$, and the driving frequency of F_b is ω_L. The g and J express the second-order nonlinear strengths, which can be derived from the $\chi^{(2)}$ nonlinearity.[21]

For the convenience of our subsequent calculations and discussions, we study the dynamics of such a system in a rotating frame defined by

$$\hat{U}(t) = \mathrm{e}^{\mathrm{i}t(\omega_L 2\hat{a}^\dagger\hat{a} + \omega_L 2\hat{c}^\dagger\hat{c} + \omega_L\hat{b}^\dagger\hat{b})},$$

then we can get an effective Hamiltonian $\hat{H}_{\mathrm{eff}} = \hat{U}\hat{H}\hat{U}^\dagger - \mathrm{i}\hat{U}\,\mathrm{d}U^\dagger/\mathrm{d}t$ as follows:

$$\begin{aligned}\hat{H}_{\mathrm{eff}} = {} & \Delta_a\hat{a}^\dagger\hat{a} + \Delta_b\hat{b}^\dagger\hat{b} + \Delta_c\hat{c}^\dagger\hat{c} + J(\hat{a}^\dagger\hat{b}^2 + \hat{b}^{\dagger 2}\hat{a}) \\ & + g(\hat{c}^\dagger\hat{b}^2 + \hat{b}^{\dagger 2}\hat{c}) + F_a(\hat{a}^\dagger + \hat{a}) \\ & + F_b(\hat{b}^\dagger + \hat{b}) + F_c(\hat{c}^\dagger + \hat{c}), \quad (2)\end{aligned}$$

where $\Delta_a = \omega_a - 2\omega_L$, $\Delta_b = \omega_b - \omega_L$, and $\Delta_c = \omega_c - 2\omega_L$ represent the detunings of the modes a, b, and c, respectively. Currently, some experimental implementations of similar models have been discussed in detail.[22,44] The dynamics of the density matrix ρ of the system is governed by

$$\frac{\partial\hat{\rho}}{\partial t} = -\mathrm{i}[\hat{H},\hat{\rho}] + \kappa_a\ell(\hat{a})\hat{\rho} + \kappa_b\ell(\hat{b})\hat{\rho} + \kappa_c\ell(\hat{c})\hat{\rho}, \quad (3)$$

here the κ_a, κ_b, and κ_c represent the damping constants of cavities 1, 2, and 3, respectively. The super-operator is defined by

$$\ell(\hat{o})\hat{\rho} = \hat{o}\hat{\rho}\hat{o}^\dagger - \frac{1}{2}\hat{o}^\dagger\hat{o}\hat{\rho} - \frac{1}{2}\hat{\rho}\hat{o}^\dagger\hat{o}.$$

For convenience to calculate we set $\kappa_a = \kappa_b = \kappa_c = \kappa$. In this paper, we will analyze the UPB in the low-frequency mode b, and we use the steady-state second-order correlation function to describe the statistical properties of photons,[45,46] which can be calculated by solving the master equations numerically as

$$g^{(2)}(0) = \frac{\langle\hat{b}^\dagger\hat{b}^\dagger\hat{b}\,\hat{b}\rangle}{\langle\hat{b}^\dagger\hat{b}\rangle^2}. \quad (4)$$

The $g^{(2)}(0) \ll 1$ indicates that the UPB occurs in mode b.

3. Analytical and numerical results

3.1. Analytic calculation of the system

Next, we will analyze the system analytically, and according to the system Hamiltonian, the wave function can be written as

$$\begin{aligned}|\psi\rangle = {} & C_{000}|000\rangle + C_{100}|100\rangle + C_{010}|010\rangle + C_{001}|001\rangle \\ & + C_{020}|020\rangle. \quad (5)\end{aligned}$$

This is a good approximation when we restrict the system containing a single photon with high frequency.[43] Here $|mnp\rangle$ denotes the Fock-state basis of the system with the photon numbers m, n, and p in modes a, b, and c, respectively. Consider environmental influence we can treat the system by the non-Hermitian Hamiltonian

$$\widetilde{H} = \hat{H}_{\mathrm{eff}} - \mathrm{i}\frac{\kappa}{2}\hat{a}^\dagger\hat{a} - \mathrm{i}\frac{\kappa}{2}\hat{b}^\dagger\hat{b} - \mathrm{i}\frac{\kappa}{2}\hat{c}^\dagger\hat{c}. \quad (6)$$

The $\hat{H}_{\rm eff}$ is given in Eq. (2). Substituting the wave function shown in Eq. (5) and non-Hermitian Hamiltonian into the Schrödinger equation $\mathrm{i}\partial_t|\psi\rangle = \widetilde{H}|\psi\rangle$, we can obtain the coupled equations for the coefficients

$$\begin{aligned}
\mathrm{i}\dot{C}_{000} &= F_bC_{010} + F_aC_{100} + F_cC_{001},\\
\mathrm{i}\dot{C}_{100} &= F_aC_{000} + \left(\Delta_a - \frac{\mathrm{i}\kappa}{2}\right)C_{100} + \sqrt{2}JC_{020},\\
\mathrm{i}\dot{C}_{010} &= F_bC_{000} + \left(\Delta_b - \frac{\mathrm{i}\kappa}{2}\right)C_{010} + \sqrt{2}F_bC_{020},\\
\mathrm{i}\dot{C}_{001} &= F_cC_{000} + \left(\Delta_c - \frac{\mathrm{i}\kappa}{2}\right)C_{001} + \sqrt{2}gC_{020},\\
\mathrm{i}\dot{C}_{020} &= \sqrt{2}F_bC_{010} + \sqrt{2}JC_{100} + \sqrt{2}gC_{001}\\
&\quad + 2\left(\Delta_a - \frac{\mathrm{i}\kappa}{2}\right)C_{020}.
\end{aligned} \tag{7}$$

Therefore, the steady-state coefficient equation can be expressed as

$$\begin{aligned}
&F_bC_{010} + F_aC_{100} + F_cC_{001} = 0,\\
&F_aC_{000} + \left(\Delta_a - \frac{\mathrm{i}\kappa}{2}\right)C_{100} + \sqrt{2}JC_{020} = 0,\\
&F_bC_{000} + \left(\Delta_b - \frac{\mathrm{i}\kappa}{2}\right)C_{010} + \sqrt{2}F_bC_{020} = 0,\\
&F_cC_{000} + \left(\Delta_c - \frac{\mathrm{i}\kappa}{2}\right)C_{001} + \sqrt{2}gC_{020} = 0,\\
&\sqrt{2}F_bC_{010} + \sqrt{2}JC_{100} + \sqrt{2}gC_{001}\\
&\quad + 2\left(\Delta_a - \frac{\mathrm{i}\kappa}{2}\right)C_{020} = 0.
\end{aligned} \tag{8}$$

To implementing UPB the weak driving strength must be satisfied, namely F_a, F_b, $F_c \ll \kappa$, and the probability amplitude should meet the condition of $|C_{000}| \gg |C_{010}| \gg |C_{020}|$. So, we can set $|C_{020}| = 0$, $|C_{000}| = 1$, and in order to calculate conveniently, we make the $\Delta_a = \Delta_c = \Delta$. According to the above conditions we can get a solution for Eq. (8), that is,

$$(F_b^2 + F_cg + F_aJ) + \mathrm{i}(F_b^2\Delta + F_cg\Delta_b + F_aJ\Delta) = 0. \tag{9}$$

In this paper, we only consider the case $\Delta = \Delta_b = 0$,[43] and we can get a conditional equation

$$g = -\frac{F_b^2 + F_aJ}{F_c}, \tag{10}$$

which is the optimal conditions for UPB in mode b. When the optimal conditions are satisfied, the photons cannot occupy the state $|020\rangle$, which can be examined by numerical simulation.

3.2. The physical mechanism UPB implements in this system

Now, let us discuss the physical mechanism by which this system forms UPB. And the physics behind unconventional photon blockade is the effect of quantum interference between different paths. The energy-level structure and transition paths are shown in Fig. 2. There are three paths for the system to reach the two-photon state of mode b:

(i) $|000\rangle \xrightarrow{F_b} |010\rangle \xrightarrow{F_b} |020\rangle$.
(ii) $|000\rangle \xrightarrow{F_a} |100\rangle \xrightarrow{J} |020\rangle$.
(iii) $|000\rangle \xrightarrow{F_c} |001\rangle \xrightarrow{g} |020\rangle$.

When the optimal conditions for photon antibunching are satisfied, the photons come from different pathways destructive interference and the photons cannot occupy the state $|020\rangle$, that is, the UPB will occur.

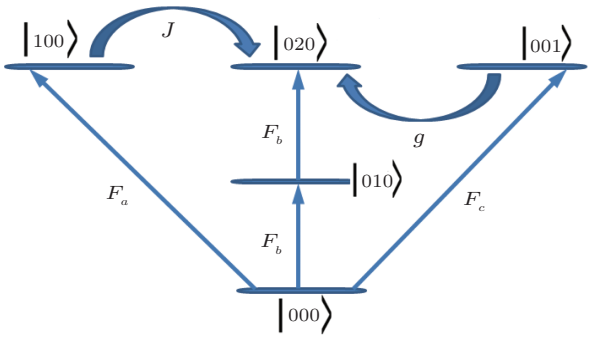


Fig. 2. Energy-level diagram. The zero-, one-, and two-photon states (horizontal short lines) and the transition paths leading to the quantum interference responsible for the UPB (The arrows indicate the interference path).

3.3. Comparative analysis of numerical and analytical solutions

In the following, we will study the UPB by the numerical simulation, and compare the results with the analytical solutions show in Eq. (10). Under a truncated Fock space we can get the second-order correlation functions via solving the master equation numerically. In the current system, the Hilbert spaces are truncated to five dimensions for cavity modes a, b, and c, respectively. For convenience, we rescale all parameters in units of the dissipation rate κ in Eq. (10), and the normalized optimal condition can be written as

$$\frac{g}{\kappa} = -\frac{(F_b/\kappa)^2 + F_aJ/\kappa^2}{F_c/\kappa}. \tag{11}$$

As is shown in Eq. (11), when the coefficient $J/\kappa = 0$, the above analytic solution is the same with that given in Ref. [43]. Next, the current system will be numerically calculated to discuss the influence of each parameter on the UPB effect. The results are shown in Fig. 3.

In Fig. 3(a), we show the logarithmic plot of $g^{(2)}(0)$ as a function of F_b/κ and g/κ, the other parameters are $F_a/\kappa = 0.01$, $F_c/\kappa = 0.01$, and $J/\kappa = 0.01$. We find that there is a parabolic dip corresponds to $g^{(2)}(0) \ll 1$, and the white dotted line represents the analytic condition from Eq. (11), which agrees well with the numerical solution. According to existing parameters and the results shown in Fig. 2(a), when the strengths of the bimodal driving are the same the UPB can

also happen, which is completely different from a system with a Kerr nonlinearity.[43] When $F_a = F_b = F_c = F$, the optimal blocking condition will be simplified as

$$g/\kappa = -(F/\kappa + J/\kappa). \tag{12}$$

In Fig. 3(b), we logarithmic plot $g^{(2)}(0)$ as a function of J/κ and g/κ for $F_a/\kappa = F_b/\kappa = F_c/\kappa = 0.01$. The numerical results show that, the UPB can occur in this system, where the valleys in $g^{(2)}(0) < 1$ correspond to the strong photon antibunching, the shape of which is similar to a slash. The analytic solution is denoted by the white dotted line, which agrees well with numerical simulations. According to the Hamiltonian and analytic solutions of the system, it is not difficult to see that the second-order nonlinear coefficients g and J are symmetric, which is consistent with the numerical results shown in the figure. In the following discussion, we will further analyze the influence of this symmetric relation on the realization of UPB effect in the system.

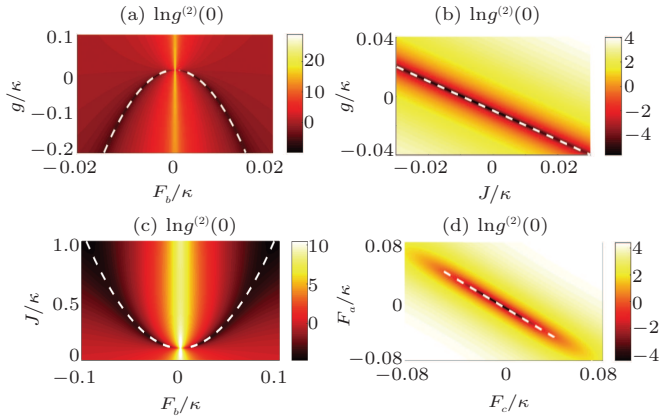


Fig. 3. (a) Logarithmic plot $g^{(2)}(0)$ as a function of F_b/κ and g/κ, and we set $F_a/\kappa = 0.01$, $F_c/\kappa = 0.01$, and $J/\kappa = 0.01$. (b) Logarithmic plot $g^{(2)}(0)$ varying with J/κ and g/κ for $F_a/\kappa = 0.01$, $F_b/\kappa = 0.01$, and $F_c/\kappa = 0.01$. (c) Logarithmic plot $g^{(2)}(0)$ as a function of F_b/κ and J/κ, and we set $F_c/\kappa = 0.01$, $F_a/\kappa = -0.01$, and $g/\kappa = 0.1$. (d) Logarithmic plot $g^{(2)}(0)$ as a function of F_c/κ and F_a/κ, and we set $F_b/\kappa = 0.02$, $g/\kappa = 0.04$, and $J/\kappa = 0.06$. In panels (a)–(d), the dashed lines represent the analytical results.

To further analyze the influence of system parameters on $g^{(2)}(0)$, in Fig. 3(c) we logarithmically plot of $g^{(2)}(0)$ as a function of F_b/κ and J/κ, and we set $F_c/\kappa = 0.01$, $F_a/\kappa = -0.01$, and $g/\kappa = 0.1$. Here, since the value of the driver term coefficient F_a/κ in Figs. 3(a) and 3(c) is opposite in sign, the shape of the photonic anticlustering region of the system implementation is opposite, which is consistent with the analytic condition in Eq. (10). It also verifies the symmetric relation between two nonlinear coupling terms in the system and the reliability of numerical simulation. In Fig. 3(c), we set $g = 0.1$. By comparison with Fig. 3(a), we found that greater nonlinearity could make F_b/κ have larger value range and make the blockade window of the system larger. In Fig. 3(d), we logarithmically plot $g^{(2)}(0)$ as a function of F_c/κ and F_a/κ, and we set $F_b/\kappa = 0.02$, $g/\kappa = 0.04$, $J/\kappa = 0.06$, and $\Delta_a = \Delta_b = \Delta_c = 0$. And the white dotted line represents the analytical results. According to the results in the figure, we find that the system can realize strong anticlustering under different driving strength combinations, and the numerical solution and analytical solution are in good agreement. At the same time, it is not difficult to find that strong photonic anticlustering regions occur in regions with small absolute values of F_a/κ and F_c/κ, which further verifies that the system must satisfy weak-driving conditions to achieve photonic anticlustering.

Next, the numerical and analytical solutions of the system will be further compared and analyzed, and we will derive an analytic calculation expression for $g^{(2)}(0)$, and then compare it with the numerical simulations. In order to approximately get the analytic solution of $g^{(2)}(0)$, we solve Eq. (8) under the weak-driving condition and the vacuum state C_{000} approximately having unit occupancy, *i.e.*, $C_{000} = 1$. We can get a new coefficient equation as

$$\begin{aligned}
&F_a + \left(\Delta_a - \frac{\mathrm{i}\kappa}{2}\right) C_{100} + \sqrt{2} J C_{020} = 0,\\
&F_b + \left(\Delta_b - \frac{\mathrm{i}\kappa}{2}\right) C_{010} + \sqrt{2} F_b C_{020} = 0,\\
&F_c + \left(\Delta_c - \frac{\mathrm{i}\kappa}{2}\right) C_{001} + \sqrt{2} g C_{020} = 0,\\
&\sqrt{2} F_b C_{010} + \sqrt{2} J C_{100} + \sqrt{2} g C_{001}\\
&\qquad + 2\left(\Delta_a - \frac{\mathrm{i}\kappa}{2}\right) C_{020} = 0.
\end{aligned} \tag{13}$$

For convenience, we set the $\Delta_a = \Delta_c = \Delta$, and then the solutions of Eqs. (13) are given as follows:

$$\begin{aligned}
C_{100} &= \frac{8\mathrm{i}J(F_b^2 + F_c g y) + 2F_a(4g^2 + xy)(-\mathrm{i}k + 2\Delta_b)}{xy(4g^2 + 4J^2 + xy)},\\
C_{010} &= \frac{-2\mathrm{i}F_b}{y},\\
C_{001} &= \frac{8\mathrm{i}F_b^2 g x + (-\mathrm{i}k + 2\Delta_b)[-4F_a g J + F_c(4J^2 + xy)]}{xy(4y^2 + 4J^2 + xy)},\\
C_{020} &= \frac{2\sqrt{2}[F_b^2 x + y(F_c g + F_a J)]}{xy(4g^2 + 4J^2 + xy)},
\end{aligned} \tag{14}$$

where the parameters $x = k + \mathrm{i}2\Delta$ and $y = k + \mathrm{i}2\Delta_b$. The $g^{(2)}(0)$ can be expressed as the probabilities of n-photon distribution function P_n as

$$g^{(2)}(0) = \frac{\sum_n n(n-1)P_n}{(\sum_n nP_n)^2}, \tag{15}$$

and under the weak pumping limit, $g^{(2)}(0)$ can be written as follows:

$$g^{(2)}(0) \simeq \frac{2|C_{020}|^2}{|C_{010}|^4}. \tag{16}$$

According to Eqs. (14) and (16) we can obtain the

$$g^{(2)}(0)=\frac{(F_b^2+F_cg+FaJ)^2\kappa^4}{F_b^4(4g^2+4J^2+\kappa^2)}. \tag{17}$$

In Fig. 4 we plot $g^{(2)}(0)$ *versus* various parameters, in which the red dotted line indicates the numerical solution and the blue solid line expresses the analytical solution.

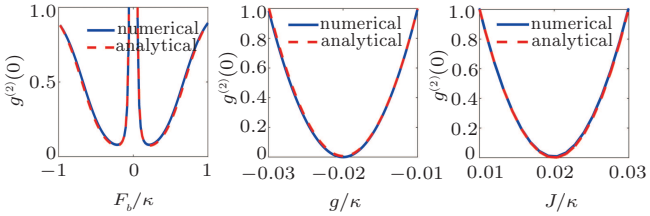


Fig. 4. We plot $g^{(2)}(0)$ as a function of F_b/κ, g/κ, and J/κ. In panel (a) we set $F_a/\kappa=0.01$, $F_c/\kappa=0.1$, $J/\kappa=0.3$, and $g/\kappa=0.3$. In panel (b) $F_a/\kappa=0.01$, $F_b/\kappa=0.01$, $F_c/\kappa=-0.01$, and $g/\kappa=0.01$. In panel (c) $F_a/\kappa=0.01$, $F_b/\kappa=0.01$, $F_c/\kappa=0.01$, and $J/\kappa=0.01$. In panels (a)–(c) the dashed lines indicate the analytical results.

In Fig. 4(a), we plot $g^{(2)}(0)$ *versus* F_b/κ, here $F_a/\kappa=0.01$, $F_c/\kappa=0.1$, $J/\kappa=0.3$, $g/\kappa=0.3$. The precise numerical solution is in good agreement with the analytical solution, and the minimum value of $g^{(2)}(0)$ appears at position $F_b/\kappa=\pm0.16$. All the results agree well with that predicted results based on the optimal blockade condition shown in Eq. (11). In Fig. 4(b), we plot $g^{(2)}(0)$ with the nonlinear interaction strength g/κ, where $F_a/\kappa=0.01$, $F_b/\kappa=0.01$, $F_c/\kappa=0.01$, and $J/\kappa=0.01$. The numerical solution agrees well with the analytical solution. According to the optimal analytic condition of Eq. (11) the optimum blockade position should appear at $g/\kappa=-0.02$, which is in perfect agreement with the graph. In order to analyze the symmetry of the system, in Fig. 4(c), we plot the $g^{(2)}(0)$ *versus* the nonlinear interaction strength J/κ, with $F_a/\kappa=0.01$, $F_b/\kappa=0.01$, $g/\kappa=0.01$, and $F_c/\kappa=-0.01$. Here, we set the driving term coefficient $F_c/\kappa=-0.01$, which is the opposite of F_a/κ and F_b/κ. The strong UPB effect still exists, and according to the optimal analytic condition, the perfect blocking position happens at $J/\kappa=0.02$, which is in good agreement with analytical conditions. Moreover, by comparing Fig. 4(b) with Fig. 4(c), we can find that the expression of the curves are the same, and the perfect blockade point has the same absolute value, which further verifies the symmetric relationship between g and J in the system, and it agrees well with the results shown in Fig. 3(b).

Next, we discuss the effect of dissipation rate κ and driving strength on UPB in the current system. Firstly, according to the optimal condition for strong antibunching in Eq. (10), the κ does not appear in the expression for the analytic condition, so, in theory, κ has no effect on the position of optimal conditions. In Fig. 4(a) we plot $g^{(2)}(0)$ *versus* κ. In the black solid line we set $F_a/\kappa=F_b/\kappa=F_c/\kappa=0.01$, $J/\kappa=0.5$, and the value of g/κ is calculated by Eq. (10). As $g/\kappa=-0.51$, strong UPB occurs in the black solid line, and the effect of UPB does not change significantly when κ varies over a large range, and the same thing happens in the blue dotted line and red point line in Fig. 5(a). So, the UPB effect is insensitive to κ in this system, and the results are consistent with that of theoretical prediction. Secondly, in order to realize UPB theoretically, the condition of weak driving must be satisfied, so we plot $g^{(2)}(0)$ *versus* the dissipation rate κ under different driving strengths. For convenience, we set the driving strengths $F_a=F_b=F_c=F$ in three lines, and in the blue dotted line the parameter are $F/\kappa=0.1$, $J/\kappa=0.5$ and according to optimal blocking condition $g/\kappa=-0.6$, and in the red point line $F/\kappa=1$, $J/\kappa=0.5$, and $g/\kappa=-1.5$. By comparing these three curves we can find the UPB effect occurs in all three curves, but the blocking effect decreased significantly with the increase of F/κ, which agrees well with theoretical prediction. In the previous researches, we studied the UPB effect at zero temperature, and now we will investigate the UPB effect at nonzero temperatures. In order to discuss effect of temperature on UPB, we need to redefine the density matrix $\hat{\rho}$ for this system as follows:

$$\begin{aligned}\frac{\partial\hat{\rho}}{\partial t}=&-\mathrm{i}[\hat{H},\rho]+\frac{\kappa_a}{2}(\bar{n}_{\mathrm{th}}+1)(2\hat{a}\hat{\rho}\hat{a}^\dagger+\hat{a}^\dagger\hat{a}\hat{\rho}+\hat{\rho}\hat{a}^\dagger\hat{a})\\&+\frac{\kappa_b}{2}(\bar{n}_{\mathrm{th}}+1)(2\hat{b}\hat{\rho}\hat{b}^\dagger+\hat{b}^\dagger\hat{b}\hat{\rho}+\hat{\rho}\hat{b}^\dagger\hat{b})\\&+\frac{\kappa_c}{2}(\bar{n}_{\mathrm{th}}+1)(2\hat{c}\hat{\rho}\hat{c}^\dagger+\hat{c}^\dagger\hat{c}\hat{\rho}+\hat{\rho}\hat{c}^\dagger\hat{c})\\&+\frac{\kappa_a}{2}\bar{n}_{\mathrm{th}}(2\hat{a}^\dagger\hat{\rho}\hat{a}+\hat{a}\hat{a}^\dagger\hat{\rho}+\hat{\rho}\hat{a}\hat{a}^\dagger)\\&+\frac{\kappa_b}{2}\bar{n}_{\mathrm{th}}(2\hat{b}^\dagger\hat{\rho}\hat{b}+\hat{b}\hat{b}^\dagger\hat{\rho}+\hat{\rho}\hat{b}\hat{b}^\dagger)\\&+\frac{\kappa_c}{2}\bar{n}_{\mathrm{th}}(2\hat{c}^\dagger\hat{\rho}\hat{c}+\hat{c}\hat{c}^\dagger\hat{\rho}+\hat{\rho}\hat{c}\hat{c}^\dagger).\end{aligned} \tag{18}$$

In Fig. 5(b), we logarithmically plot $g^{(2)}(0)$ as a function of F_a/κ under different numbers of thermal photons $\bar{n}_{\mathrm{th}}$, where $F_b/\kappa=0.01$, $F_c/\kappa=0.01$, $J/\kappa=0.01$, and $g/\kappa=0.01$ are the same in these three lines, and in the black solid line we set $\bar{n}_{\mathrm{th}}=0$, in the blue dotted line $\bar{n}_{\mathrm{th}}=0.05$, in the red point line $\bar{n}_{th}=0.1$. The results show that the strongest UPB point appears on $F_a/\kappa=1.3$, just as predicted. Moreover, when $\bar{n}_{\mathrm{th}}$ changes in a larger range, the UPB effect does not change significantly, which indicates that this scheme is not sensitive to the change of the reservoir temperature, that makes the system easier to implement experimentally.

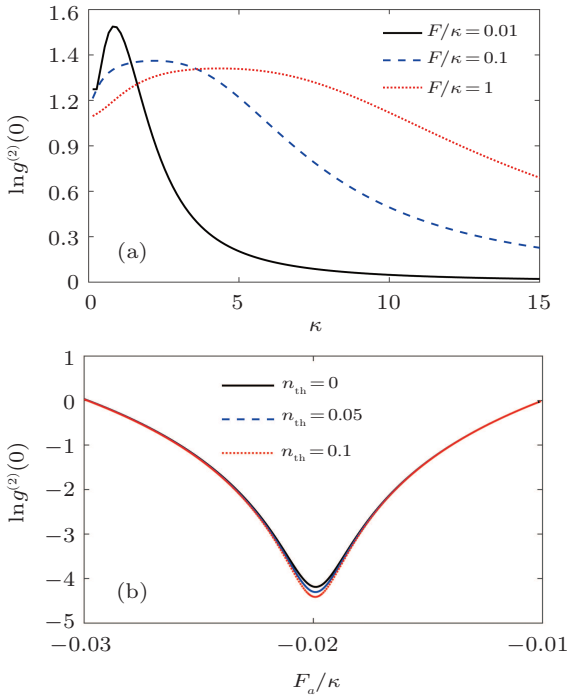


Fig. 5. (a) Under different driving strengths we plot $g^{(2)}(0)$ *versus* the dissipation rate κ, and consider the optimal blocking condition in the black solid line $F_a/\kappa = F_b/\kappa = F_c/\kappa = 0.01$, $J/\kappa = 0.5$, and $g/\kappa = -0.51$, in the blue dotted line $F_a/\kappa = F_b/\kappa = F_c/\kappa = 0.1$, $J/\kappa = 0.5$, and $g/\kappa = -0.6$, and in the red point line $F_a/\kappa = F_b/\kappa = F_c/\kappa = 1$, $J/\kappa = 0.5$, and $g/\kappa = -1.5$. (b) Under different numbers of thermal photons $\bar{n}_{\rm th}$ logarithmically we plot $g^{(2)}(0)$ *versus* the driving strength F_a/κ, with $F_b/\kappa = 0.01$, $F_c/\kappa = 0.01$, $J/\kappa = 0.01$, and $g/\kappa = 0.01$, which are the same in these three lines, and in the black solid line we set $\bar{n}_{\rm th} = 0$, in the blue dotted line $\bar{n}_{\rm th} = 0.05$, in the red point line $\bar{n}_{\rm th} = 0.1$. Panels (a) and (b) are numerical results.

In the following, we discuss the difference between the current system and the two-mode second-order nonlinear system[43] in realizing the UPB effect. In Fig. 6(a) we logarithmically plot $g^{(2)}(0)$ as a function of g/κ under different J/κ, and in the black curve, we set the system parameters as $F_b/\kappa = 0.01$, $F_c/\kappa = -0.01$, $F_a/\kappa = 0.01$, and $J/\kappa = 0.01$, and in the red curve $F_b/\kappa = 0.01$, $F_c/\kappa = -0.01$, $F_a/\kappa = 0.01$, and $J/\kappa = 0$. When the second-order nonlinear coefficient $J/\kappa = 0$, the current system is the same as the two-mode system,[43] and the blockaed conditions are the same. According to the results shown in Fig. 6(a), under the same weak driving condition, the UPB effect of the double second-order nonlinear system is more obvious, which may be mainly due to the addition of a second-order nonlinear coupling term in the current system. That forms a symmetric interference path and makes the destructive quantum interference more obvious. To further discuss the advantages of the current system in realizing CPB effect, in Fig. 6(b) we logarithmically plot $g^{(2)}(0)$ as a function of g/κ under different J/κ, and in the black curve, we set the system parameter as $F_b/\kappa = 0.1$, $F_c/\kappa = -0.1$, $F_a/\kappa = 0.1$, and $J/\kappa = 0.01$, and in the red curve $F_b/\kappa = 0.1$, $F_c/\kappa = -0.1$, $F_a/\kappa = 0.1$, and $J/\kappa = 0$. As shown in Fig. 6(b), when the driving strength of the system increases, the effect of the system to achieve UPB effect is significantly weakened. However, consistent with the results in Fig. 6(a), the extreme value of $g^{(2)}(0)$ of the double second-order nonlinear system is smaller.

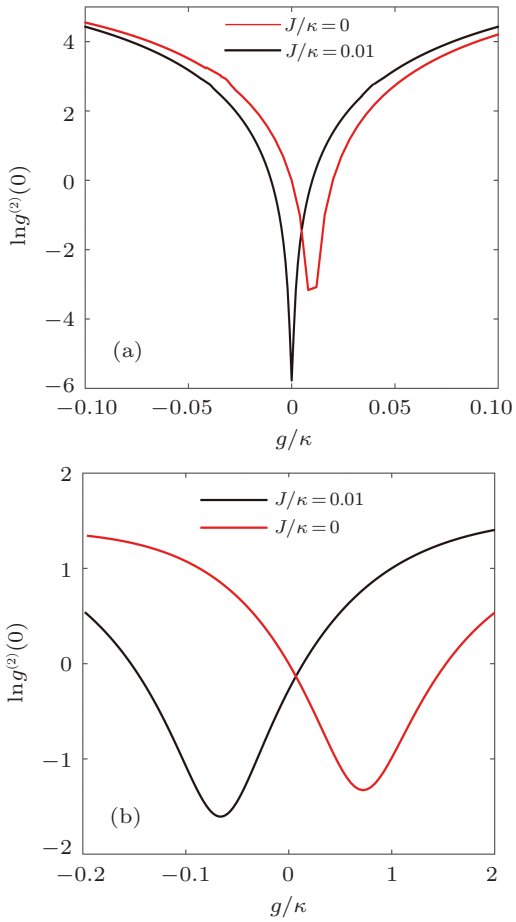


Fig. 6. (a) Logarithmic plot of $g^{(2)}(0)$ *versus* g/κ, in the black curve we set $F_b/\kappa = 0.01$, $F_c/\kappa = -0.01$, $F_a/\kappa = 0.01$, and $J/\kappa = 0.01$ and in the red curve $F_b/\kappa = 0.01$, $F_c/\kappa = -0.01$, $F_a/\kappa = 0.01$, and $J/\kappa = 0$. (b) Logarithmic plot of $g^{(2)}(0)$ *versus* g/κ, in the black curve we set $F_b/\kappa = 0.1$, $F_c/\kappa = -0.1$, $F_a/\kappa = 0.1$, and $J/\kappa = 0.01$ and in the red curve $F_b/\kappa = 0.1$, $F_c/\kappa = -0.1$, $F_a/\kappa = 0.1$, and $J/\kappa = 0$. Both of panels (a) and (b) are numerical results.

Finally, we discuss the difference between the current system and another similar three-mode system described in Ref. [47] in the realization of UPB effect where two high-frequency modes are linearly coupled, and one of the high-frequency modes is coupled with one low-frequency mode by second-order nonlinear materials. In Fig. 7, we logarithmically plot $g^{(2)}(0)$ as a function of g/κ under similar system parameters. The red dotted line represents the current system, and the black solid line represents the system studied in Ref. [47]. In the red dotted line we set the high-frequency mode driver $F_a/\kappa = -0.01$ and $F_c/\kappa = 0.01$, the low-frequency mode driver $F_b/\kappa = 0.1$ and $J/\kappa = 0.1$. In the black solid line we set the high-frequency mode driver $F_b/\kappa = -0.01$, and the low-frequency mode driver $F_c/\kappa = 0.1$ and $J/\kappa = 0.1$. According to the results shown in Fig. 7,

UPB occurs in both of the two systems, but the UPB effect is stronger in the current system under a small second-order nonlinear coefficient g.

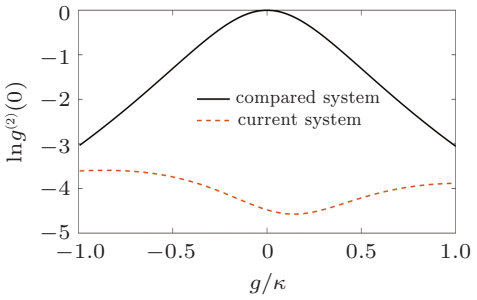


Fig. 7. Under similar system parameters, we draw a logarithmic plot of $g^{(2)}(0)$ *versus* g/κ, the red dotted line represents the current system, and the black solid line represents the system studied in Ref. [47]. In the red dotted line we set the high-frequency mode driver $F_a/\kappa = -0.01$ and $F_c/\kappa = 0.01$, the low-frequency mode driver $F_b/\kappa = 0.1$, $J/\kappa = 0.1$, and $\Delta_a = \Delta_b = \Delta_c = 0$. In the black solid line we set the high-frequency mode driver $F_b/\kappa = -0.01$, and the low-frequency mode driver $F_c/\kappa = 0.1$, $J/\kappa = 0.1$, and $\Delta_a = \Delta_b = \Delta_c = 0$.

4. Conclusion

In this paper, we investigated the unconventional photon blockade in a three-mode system with double second-order nonlinear coupling terms. We obtained the strong photon anti-bunching conditions for low-frequency mode both analytically and numerically. According to comparisons of analytical simulation and numerical calculations, the two results are in good agreement. Through the numerical analysis of the system, we find that the weak driving strength is favorable for the system to realize the UPB effect, and the system is insensitive to the changes of attenuation rate and environmental temperature. By analyzing the symmetric relation of two second-order nonlinear terms in the system, we find that this symmetric relation is more likely to produce destructive quantum interference to realize UPB effect. And by comparing with the two-mode system and another similar three-mode system, we obtain that this double second-order nonlinear system can achieve UPB more obviously under similar system parameters.

References

[1] Scarani V, Bechmann P H and Peev M 2009 *Rev. Mod. Phys.* **81** 1301
[2] Giovannetti V, Lloyd S and Maccone L 2011 *Nat. Photon.* **5** 222
[3] Knill E, Lafiamme R and Milburn G J 2001 *Nature* **409** 46
[4] Shields A J 2007 *Nat. Photon.* **1** 215
[5] Davidovich L 1996 *Rev. Mod. Phys.* **68** 127
[6] Buluta I, Ashhab S and Nori F 2011 *Rep. Prog. Phys.* **74** 104401
[7] Lang C, Bozyigit D and Eichler C 2011 *Phys. Rev. Lett.* **106** 243601
[8] Hofiman A J, Srinivasan S J, Schmidt S, Spietz L, Aumentado J and Houck A A 2011 *Phys. Rev. Lett.* **107** 053602
[9] Ferretti S, Andreani L C and Gerace D 2010 *Phys. Rev. A* **82** 013841
[10] Liao J Q and Law C K 2010 *Phys. Rev. A* **82** 053836
[11] Miranowicz A, Paprzycka M, Liu Y X, Bajer J and Nori F 2015 *Phys. Rev. A* **87** 023809
[12] Xie H, Lin G W, Chen X, Chen Z H and Lin X M 2016 *Phys. Rev. A* **93** 063860
[13] Liu Y C, Hu Y W, Wong C W and Xiao Y F 2013 *Chin. Phys. B* **22** 114213
[14] Chen X, Liu X W, Zhang K Y, Yuan C H and Zhang W P 2015 *Acta Phys. Sin.* **64** 164211 (in Chinese)
[15] Chen H J and Mi X W 2011 *Acta Phys. Sin.* **60** 124206 (in Chinese)
[16] Zhang D and Zheng Q 2013 *Chin. Phys. Lett.* **30** 024213
[17] Jiang C, Cui Y and Li X 2016 *Chin. Phys. B* **25** 054204
[18] Imamoglu A, Schmidt H, Woods G and Deutsch M 1997 *Phys. Rev. Lett.* **79** 1467
[19] Lin H Y, Wang X Q, Yao Z H and Zou D D 2020 *Opt. Express* **28** 17643
[20] Bennett S D, Stannigel K, Habraken S J M, Rabl P, Zoller P and Lukin M D 2013 *Phys. Rev. A* **87** 013839
[21] Majumdar A and Gerace D 2013 *Phys. Rev. B* **87** 235319
[22] Shen H Z, Zhou Y H and Yi X X 2014 *Phys. Rev. A* **90** 023849
[23] Shen H Z, Zhou Y H and Yi X X 2015 *Phys. Rev. A* **91** 063808
[24] Wang C Q 2012 *Chin. Phys. Lett.* **29** 084209
[25] Chang D E, Sorensen A S, Demler E A and Lukin M D 2007 *Nat. Phys.* **3** 807
[26] Gerace D, Tureci H E, Giovannetti V and Fazio R 2009 *Nat. Phys.* **5** 281
[27] Fratini F, Mascarenhas E, Safari L, Poizat J P, Valente D, Gerace D and Santos M F 2014 *Phys. Rev. Lett.* **113** 243601
[28] Mascarenhas E, Gerace D, Valente D, Montangero S and Santos M F 2014 *Europhys. Lett.* **106** 54003
[29] Liew T C H and Savona V 2010 *Phys. Rev. Lett.* **104** 183601
[30] Bayer M, Gutbrod T, Reithmaier J P, *et al.* 1998 *Phys. Rev. Lett.* **81** 2582
[31] Rakovich Y P and Donegan J F 2010 *Laser Photon. Rev.* **4** 179
[32] Shen H Z, Xu S, Zhou Y H, Wang G and Yi X X 2018 *J. Phys. B: At. Mol. Opt. Phys.* **51** 035503
[33] Ni H, Liang C H, Wang F, Chen Y H, Ponomarenko S A and Cai Y J 2020 *Chin. Phys. B* **29** 064203
[34] Li H, Zhang S Q, Guo M, Li M X and Song L J 2019 *Acta Phys. Sin.* **68** 124203 (in Chinese)
[35] Shi H Q, Xie Z Q, Xu X W and Liu N H 2018 *Acta Phys. Sin.* **67** 044203 (in Chinese)
[36] Zhang W, Yu Z Y, Liu Y M and Peng Y W 2014 *Phys. Rev. A* **89** 043832
[37] Bamba M and Ciuti C 2015 *Appl. Phys. Lett.* **99** 171111
[38] Xu X W and Li Y J 2013 *J. Phys. B: At. Mol. Opt. Phys.* **46** 035502
[39] Ferretti S, Savona V and Gerace D 2013 *New J. Phys.* **15** 025012
[40] Flayac H and Savona V 2013 *Phys. Rev. A* **88** 033836
[41] Gerace D and Savona V 2014 *Phys. Rev. A* **89** 031803
[42] Flayac H and Savona V 2017 *Phys. Rev. A* **95** 043838
[43] Zhou Y H, Shen H Z and Yi X X 2015 *Phys. Rev. A* **92** 023838
[44] Liu Y X, Xu X W, Miranowicz A and Nori F 2014 *Phys. Rev. A* **89** 043818
[45] Xiang G Y and Guo G C 2013 *Chin. Phys. B* **22** 110601
[46] Zhang L J and Xiao M 2013 *Chin. Phys. B* **22** 110310
[47] Zhou Y H, Wu Q C, Ye B L, Xue L Y and Shen H Z 2019 *Int. J. Theor. Phys.* **58** 472